Contrasting recruitment of skin-associated adipose depots during cold challenge of mouse and human

Ildiko Kasza[1], Jens-Peter Kühn[2], Henry Völzke[3], Diego Hernando[4,5],

Yaohui G. Xu[6], John W. Siebert[7], Angela LF Gibson[7],

C.-L. Eric Yen[8], David W. Nelson[8], Ormond A. MacDougald[9], Nicole E. Richardson[10,11],

Dudley W. Lamming[10,11], Philip A. Kern[12] and CM Alexander[1]*

[1]McArdle Laboratory for Cancer Research, University of Wisconsin-Madison, [2]Institute and Policlinic of Diagnostic and Interventional Radiology, Medical Faculty Carl Gustav Carus, Technical University Dresden, Germany; [3]Institute of Community Medicine, University of Greifswald, Germany; Departments of [4]Radiology, [5] Medical Physics, [6]Dermatology, [7]Surgery, [10]Medicine, University of Wisconsin-School of Medicine and Public Health; [8]Department of Nutritional Sciences, University of Wisconsin-Madison; [9]Department of Molecular & Integrative Physiology, University of Michigan; [11]William S. Middleton Memorial Veterans Hospital, Madison, Wisconsin; [12]Department of Internal Medicine, University of Kentucky, Lexington.

* corresponding author: CM Alexander, McArdle Laboratory for Cancer Research, University of Wisconsin-Madison, 1111 Highland Ave, Madison WI 53705-2275. Ph: 608-265 5182; cmalexander@wisc.edu

Running title: Human versus mouse skin associated fat

Abbreviations: dWAT, dermal white adipose tissue; scWAT, subcutaneous white adipose tissue; BAT, brown adipose tissue; SAF, skin-associated fat; iWAT, inguinal (subcutaneous) white adipose tissue; vWAT, visceral white adipose tissue; MRI, magnetic resonance imaging

Keywords: Dermal white adipose tissue; dWAT; thermogenesis; obesity; subcutaneous white adipose tissue; scWAT; UCP1; lipolysis; β-adrenergic response; skin-associated fat

Conflict of interest statement: The University of Greifswald is a member of the 'Center of Knowledge Interchange' program of Siemens AG. Contrast-enhanced MRI research is part of the entire whole-body MRI study and was supported by Bayer Healthcare. The content of the manuscript is solely the responsibility of the authors and does not necessarily represent the official views of the NIH. This work does not represent the views of the Department of Veterans Affairs or the United States Government.

Abstract. Mammalian skin impacts metabolic efficiency system-wide, controlling the rate of heat loss and consequent heat production. Here we compare the unique fat depots associated with mouse and human skin, to determine whether they have corresponding function and regulation. For human, we distinguish skin-associated fat (SAF) as the body-wide depot and characterize it separately from the subcutaneous fat pads characteristic of abdomen and upper limbs. We show that the thickness of SAF is not related to general adiposity; it is much thicker (1.6-fold) in women than men, and highly subject-specific. We used molecular and cellular assays of β-adrenergic induced lipolysis and found that dermal white adipose tissue (dWAT) in mice is resistant to lipolysis; in contrast, the body-wide human SAF depot becomes lipolytic, generating heat in response to β-adrenergic stimulation. In mice challenged to make more heat to maintain body temperature (either environmentally or genetically), the thickness of dWAT increases, whereas β-adrenergic stimulation reduces the size of human skin-associated adipocytes. We summarize the regulation of the skin-associated adipocytes by age, sex, and adiposity, for both species, and conclude that overall, a combination of subcutaneous and dermal adipose tissues in mouse contributes the same way to maintaining body temperature as human SAF.

Introduction

Specializations of mammalian adipose depots determine their individual impact on human health (1-6). In general, obesity is associated with metabolic abnormalities and the development of a variety of diseases, from diabetes to cancer, yet not all large deposits of adipose tissue types are linked to disease susceptibility (7). For example, intraperitoneal visceral adipose tissue (vWAT) is linked to cardiometabolic risk, whereas accumulation of subcutaneous white adipose tissue (scWAT), especially gluteofemoral adipose in the lower body, appears to protect subjects from these health risks (3, 8).

Studies of scWAT typically describe the gluteofemoral and/or abdominal depots; however, even high-resolution techniques such as magnetic resonance imaging (MRI) tend to overlook the body-wide fat layer underneath with skin. Our studies have drawn attention to this depot; indeed a preliminary calculation suggested that this body-wide depot comprised at least half of the fat for the average lean woman (9).

The term "subcutaneous white adipose tissue" is an umbrella term that has been used differently by previous studies, and is likely to include a heterogeneous set of depots and adipocyte cell types (5, 10-14). For this study we therefore distinguish a body-wide depot (**skin-associated fat, SAF)** from **subcutaneous fat pads (sc fat pads; Fig. 1A).** SC fat pads accumulate around the abdomen and upper limbs, particularly in over-weight women with gynoid (pear-shaped) fat deposition (15, 16), and they have been quantified by MRI (17). Our goal is to specifically examine the behavior, properties and regulation of SAF; given its size and location, we hypothesize that SAF could impact system-wide metabolism and energy balance.

In particular, we are focused on the thermal defense properties of mouse and human skin-associated fat. Thus, a layer of fat, applied body-wide to skin, is predicted to impact heat transfer properties dramatically. In turn, this affects the metabolic budget and energy expenditure of mammals; for example, mice housed at temperatures 10°C less than their thermoneutral temperature show a 50% increase in energy expenditure (18-20). The dramatic physiological cost of heat production has not gone unnoticed; a major research effort has been directed to devising a strategy for treating the epidemic rates of obesity in westernized populations, by

stimulating thermogenic adipose depots (beige/brown) to “burn” calories, using either direct cold exposure or β-adrenergic agonists (6, 21-24).

Our previous studies have shown that the skin-associated fat depot of mice (dermal white adipose tissue, dWAT) is highly regulated in a manner that suggests that this depot is part of an acclimation process that mitigates heat loss (25). Thus dWAT thickens in mice housed at room temperature (sub-thermoneutral); mice that are unable to develop thicker dWAT are chronically cold stressed (18). Importantly, several mouse strains with defects of skin lipogenic enzymes lose heat at high rates; interestingly, these strains are also resistant to diet-induced obesity (26-31).

Here, we have visualized and quantified the body-wide adipose depot associated with skin for mice and humans, running a series of comparisons that illustrate which features are shared and which are unique. By comparing the molecular properties of the adipocytes associated with mouse and human skin, we find that mouse dWAT hypertrophies when exposed to thermogenic stimuli, where human SAF become lipolytic and produces heat. Given that the amount of skin-associated fat is unique to any given individual, we propose that this could be an important and independent variable able to regulate total energy expenditure in humans.

Results

To distinguish only the skin-associated body wide depot (**SAF**), we used chemical shift MRI of lower limb, with fat/water separation (**Fig. 1B**). Fat-only images allow quantitative evaluation of fat content and SAF thickness, compared to the more standard fat/water MRI images (Fig. S1A).

In a previous pilot study we found that SAF thickness was highly variable from subject to subject, and surprisingly, not related to body mass index (or other indices of obesity such as waist/height) (9). Here, we assessed MRI images of volunteers recorded as part of a large public health study (Study of Health in Pomerania, SHIP3), including 286 women and 236 men. We found that women had thicker SAF than men (10.05±2.45 compared to 6.27±1.89 mm; **Fig.1C**). Indeed, the SAF thickness for the top decile of women was 15.0 mm, versus 6.5 mm in the bottom decile; this translates to a total predicted weight of **24.3 kg** for women with the thickest SAF layer, versus **10.5 kg** for women with the thinnest SAF, approximated using the surface area (1.8m^2) of the average woman (9). For men, this range was 9.6 mm to 3.0 mm thick (15.5-4.9 kg).

We assessed whether the thickness of SAF depended upon general adiposity, dividing the cohorts into three, lean (BMI <25), overweight (BMI 25-30) and obese (BMI >30; **Fig. 1C**). SAF did not thicken significantly in obese or over-weight men. For women, there was only a minor correlation between BMI and thicker SAF (r^2=0.10) for lean versus overweight women (9.00± 1.73 compared to 10.41±2.49 mm); this did not increase further for the obese cohort (**Fig. 1D**).

We tested the distributions of values for SAF thickness for men and women, and found that for men, the values were normally distributed; for women, the values were not, best fitting a lognormal distribution, and tailing towards thicker SAF (**Fig. 1C,** S1B,C). This implies an independent factor that promotes the accumulation of SAF in a minority of women. Perhaps surprisingly, we noted no significant correlation of SAF thickness with age, for either men or women (55 men and 57 women over 70; **Fig. 1E**).

To assess similarities and differences between mouse and human skin-associated adipose depots, we first describe their morphology and anatomy. Mouse dermal white adipose tissue (dWAT) is clearly demarcated by

a muscle layer (*panniculus carnosus*), making it simple to distinguish from the subcutaneous depots of the mammary glands (females) or mammary fat pads (males) (25). The most commonly studied scWAT depot in mouse is the inguinal fat pad, or iWAT; this is immediately subjacent to the dWAT layer (proximity is illustrated in **Fig. 8**).

Overall, the thickness of dWAT varies from almost zero (young C57BL/6J males or rats) to 400 μm, typical of anagen stage dorsal skin for BALB/cJ mice, or obese mice (**Fig. 2A,B,D,E**). The average thickness for non-anagen stage dorsal skin from chow-fed adult BALB/cJ females housed in room temperature housing is 350 μm (**Fig.2D**).

We noticed that dWAT accumulates steeply in C57BL/6J males between the ages of 20 and 30 weeks; this occurs prior to, and during, a phase of rapid continuous body weight gain (**Fig. 2B**).

Using an immunohistochemical stain to outline the fat globule of adipocytes (anti-perilipin), we found that mouse dermal adipocytes contain approximately the same amount of fat as inguinal/subcutaneous WAT adipocytes, but only half the amount of fat in visceral adipocytes (measured as surface area; **Fig. 2C**).

We compared the thickness of dWAT in males and females from two strains, C57BL/6J and BALB/cJ mice, and found that BALB/cJ mice showed a dramatic sex dimorphism, where dWAT was almost 4x thicker in females than males (**Fig. 2D**). This was not observed for mature male and female C57BL/6J mice.

Bearing in mind the lack of correlation between human SAF thickness and obesity, we tested the impact of obesogenesis on mouse dWAT, and found that dWAT thickness expanded by 4-fold after 2 weeks of high fat feeding in for C57BL/6J males, in parallel with vWAT depots (**Fig. 2E** and Kasza et al 2016 (9)). Likewise, genetically obese mice (A^y/a) showed thick dWAT and increased dermal adipocyte size; diameters of dermal adipocytes (obese and lean) are summarized in **Table 1.**

Inflammation of obese adipose depots is linked to metabolic deterioration, and adipose depots from obese mice are differentially sensitive to invasion by inflammatory macrophages, assayed by the accumulation of crown-

like structures (CLS) (32). Given the large volume of dWAT, we investigated whether CLS appeared in dWAT depots in skins from mice fed with high-fat diets (compared to either iWAT or gWAT) and found that this depot was relatively resistant to this type of inflammation. Some crown-like structures appeared in mice genetically altered to have life-long obesity (32 week-old A^y mice; **Fig. S2A**).

Vice versa, calorie restricted mice showed depleted dWAT. We used a moderate, 25% calorie restriction protocol to assess impact on both C57BL/6J and BALB/cJ mice; this protocol induced a significant loss of body weight within 2 weeks. After 4 weeks of calorie restriction, C57BL/6J mice lost 18% body weight, and BALB/cJ mice lost 22% body weight (**Fig. 3A**). DWAT mirrored the loss of body weight; both strains lost >100 μm thickness of dWAT (**Fig. 3B**), so the leanest calorie restricted BALB/cJ mice showed negligible dWAT levels after 4 weeks (**Fig. S2B**).

In contrast, human subcutaneous adipose tissues comprise capsules of yellow fat attached to the dermis/epidermis; capsule size ranges from 5-15 mm, where the lipid-filled adipocytes are encapsulated by thick seams of collagen (**Fig. 4A**). Several publications have reviewed the topic of potential heterogeneity of human subcutaneous adipose tissue (13, 14, 17, 33, 34); in particular, deep layers of skin-associated fat may have different properties compared to the more superficial layers (35, 36). We found little difference in the size of adipocytes from superficial (within 2 mm of dermis), mid (2-12 mm) and deeper layers (more than 12 mm from dermis; n=7) for samples from lean individuals (**Fig. 4A,B**); neither did we observe significant differences in adipocyte sizes from different body locations (for example breast versus lower body (thigh) versus upper body (abdominal); n=7, 4, 5 respectively) (**Fig. 4B,C**). The adipocytes from visceral depots and breast and abdominal subcutaneous sites all underwent hypertrophy (**Fig. 4C**). In summary, human subcutaneous adipocytes of lean subjects were larger on average (56 um diameter) than mouse dermal adipocytes (40 um diameter), and adipocytes from both human and mouse undergo hypertrophy during obesogenesis (67 and 59 um respectively; **Fig. 4D; Table 1**).

Human and mouse subcutaneous adipose depots are typically ascribed a supportive role in the thermogenic response; they are activated by β-adrenergic agents to become lipolytic, to provide fatty acid fuels for heat

production by BAT, or to participate in the beiging response (37-39). However, the analysis of the transcriptome of mouse dermal adipocytes performed by Scherer and colleagues suggested that this population was unlike adipocytes in brown or beiging depots, resembling vWAT instead (40); they showed that dWAT showed no lipid depletion upon treatment with a β-adrenergic agent (scored as a reduction from mono- to multi-locularity of the lipid body).

To further evaluate the molecular response of dermal white adipocytes to cold stress, we evaluated the regulatory modification of hormone-sensitive lipase (HSL) in response to the β-adrenergic agonist CL *in vivo* using an immunohistochemical assay (**Fig. 5**). HSL is part of a complex that integrates input stimuli from kinases to coordinate lipolysis brown adipose tissue (41, 42). We confirmed the accuracy of HSL (and FASN) stains using mouse adipocyte cultures treated with the pan β-adrenergic agonist, isoproterenol (**Fig. S3**). Tissue samples of BAT and iWAT showed a gain of signal for the PKA-dependent activating phosphorylation of S^{660} (**pHSL stim**), whereas vWAT showed a gain of signal for the AMPK-dependent inhibitory phosphorylation of S^{565} (**pHSL inh**; **Fig. 5A, B**). Positive staining for fatty acid synthase, FASN, and fatty acid binding protein-4, FABP4, was suppressed in iWAT and BAT, and unchanged/negative for vWAT and dWAT (**Fig. S4**). This confirms that dWAT was non-responsive to β-adrenergic-induced heat production, measured by the same criteria used to assess the recruitment of brown and beige depots.

To corroborate this result, we tested another β-adrenergic/PKA-induced reaction; thus, activation of mTORC1 is known to be essential for β-adrenergic induced lipolysis in adipocytes (43). S6 and S6-kinase are activated and phosphorylated downstream of the mTORC1 kinase and are markers of mTORC1 activation status. Signal for phospho-$S^{240/244}$ S6 was induced in BAT and iWAT in CL-administered mice but showed no reaction in dWAT (**Fig. 5A**), despite the local activation of muscle and sebocytes by β-adrenergic stimulation. To confirm that these immunohistochemical assays reflect active lipolysis, we measured the size of adipocyte lipid stores in mice that were activated to produce heat, either by transfer to 4°C environment or 60 minutes after CL administration. We found lipid stores significantly depleted in iWAT, but not in dWAT (**Fig. 5C, S5**). In

summary, when BAT and iWAT become lipolytic in response to β-adrenergic stimulation, dWAT shows little molecular response, like vWAT and bone marrow adipocytes (44).

We hypothesized that in mice chronically stimulated to produce more heat, dWAT would instead react to mitigate heat loss. Mice housed at room temperature (19°C) compared to thermoneutral housing (31°C) show thicker dWAT (1.6x; **Fig.6A**). To test this hypothesis using a genetic model, we evaluated *UCP1-/-* mice. These mice have a lesion in the most efficient heat production mechanism (affecting the uncoupling of BAT mitochondria), and deploy instead beiging and other "non-canonical" mechanisms to compensate (45). As with environmentally cool-stressed mice, genetically cool-stressed mice also show thicker dWAT (**Fig. 6B**). This supports the claim that the accumulation of fat in dWAT is an adaptive response to environmental cooling.

What triggers this adaptive response? In particular, we noticed that mammals typically experience variation of environmental temperature over the circadian daily cycle. To begin to isolate environmental cues, we divided the housing cycle into a warm phase (thermoneutral, 31°C/88°F) and a cool phase (cool room temperature, 19°C/66°F). Although the length of time in each phase was constant for mice in cycling environments, only the mice housed cool during their sleep cycle developed thicker dWAT (**Fig. 6C**); the same cue given to awake mice did not induce dWAT thickening. This suggests that there is a component of circadian control of dWAT lipogenesis.

Turning to the molecular regulation of skin-associated fat in human, we administered β-adrenergic agonists either *in vivo* or *ex vivo,* and assayed HSL activation and lipid store mobilization. Human abdominal, breast and thigh skin-associated fat administered the pan-β adrenergic agent isoproterenol *ex vivo* showed uniform activation of HSL and lipid store depletion (**Fig. 7A, B**). Likewise, abdominal adipose tissues from obese subjects administered the β3-adrenergic agent mirabegron daily, also showed activated HSL, and higher UCP1 staining (**Fig. S6**)(46). Skin-associated fat in calf, thus the same body site imaged for the data of Fig. 1, also showed HSL activation after exposure to isoproterenol (**Fig. S7**). The β-adrenergic response was therefore a

consistent feature of human skin-associated adipose tissues, regardless of body site or distance from skin (superficial or deep).

Typically, lipolysis of subcutaneous fat is considered to have a supporting role for the delivery of fatty acids to dedicated, heat-generating organs such as brown adipose tissue or muscle. However, emerging literature suggests that a number of UCP1-independent biochemical pathways can be harnessed for the purpose of regulated heat production (47), where the substrates used to fuel oxidation are not yet clearly defined. Therefore, to directly evaluate whether β-adrenergic activation can induce heat production in skin-associated fat, we used infrared thermography (FLIR) to assay fat explants *ex vivo* and found a significant rise in temperature in response to isoproterenol treatment (**Fig. 7C**). We conclude that human skin-associated adipose tissue is an active participant in heat production, and not just a passive insulator.

Discussion

We compared the most superficial layers of adipose associated with skins of human and mouse and showed that they respond differently to the thermogenic environment; thus the dermal adipocytes associated with mouse skin are protected from lipolysis, where the skin-associated fat of human skin becomes lipolytic and directly produces heat (**Table 1**). Thus, the human skin-associated fat layer comprises a dynamically warming blanket that is able not only to resist heat loss but to produce its own heat (see scheme in **Fig. 8**). We have shown that human skin-associated adipocytes are remarkably homogeneous in their ability to recognize and respond to β-adrenergic effectors, whether from obese or lean subjects, and irrespective of body site.

This study is the first to quantify this specific human fat depot, though many MRI-based studies have reported segregated fat volumes that discriminate between for example visceral and sub-cutaneous abdominal fat (16, 17). Specific "fat-only" MRI data can be extracted from the data obtained for routine diagnostics, which are typically processed to show a combination of fat and water signals.

Other imaging strategies used for the study of thermogenesis rely on the detection of glucose uptake by ^{18}F-fluorodeoxyglucose (FDG)-PET imaging of activated fat depots in cool-exposed individuals. The SAF depot has not yet been noted by these studies (48). This could be 1) due to the relatively lower resolution of this technique and the disseminated nature of the depot, or 2) due to low glucose uptake by activated SAF. This is possible, since we do not yet understand the substrate requirements of heat production in non-BAT thermogenic tissues, but they probably include creatine and amino acids (49-51).

Note that we used the conservative terminology of "skin-associated fat" for human, given extensive literature documenting subcutaneous adipose tissues from human, potentially all different, since they were drawn from different body sites and depths from skin. However, for the functional aspect that we assayed (β-adrenergic induced lipolysis), we could find no differences to distinguish these depots, comparing upper versus lower body, or limb versus abdominal depots.

Women show thicker SAF than men, by 60% on average; by calculation this depot is 10.5-24.3 kgs, making it the largest individual adipose depot in the lean woman's body. The number of women with thick SAF is higher than that predicted from a normal distribution, and we speculate that the health and energy expenditure of this population may be significantly affected. Likewise, the females of the BALB/cJ mouse strain show much thicker dWAT than their male counterparts. Thus this depot is more prominent in females of both species.

The dWAT depot of mice correlates strongly with relative adiposity elsewhere, even from mouse to mouse in a given population. Mouse dWAT increases in obese mice, whether induced by high fat feeding, by age-induced obesity, or in mice made obese genetically, including *Agouti*^{y}, MitoNEET and *ob/ob* ((9, 31, 40) and this study). In adult mice, the majority of dWAT thickening is enabled by adipocyte hypertrophy (40).

In obese mice, we found this depot to be relatively resistant to the development of "crown-like structures"; these reflect the infiltration of inflammatory macrophages into depots containing distended adipocytes, typically highest in male mouse vWAT (32). For human subjects, subcutaneous adipose depots are significantly associated with inflammatory macrophage infiltration (35).

Vice versa, we showed that dWAT is depleted in mice subjected to calorie restriction. Trajkovski and colleagues showed that beige depots were activated in calorie restricted mice (52); this may support the hypothesis that dWAT thinning leads to higher demand for heat.

Given *ad libitum* calorie intake, we propose that mice deploy the combination of iWAT activation and dWAT thickening to meet heat production demands, notably when BAT activation is insufficient. Thus UCP1KO mice deploy a range of strategies for heat conservation and production (47), to ensure their body temperature is more resilient to change upon cool stress. As well as thicker dWAT (shown here), UCP1 KO mice show a change of vascular tone, so mice have a sustained vasoconstrictor response after minor cool stress (53). Fgf21 was shown to be an effector of iWAT activation in UCP1KO mice (45); perhaps Fgf21 is also an effector of dermal adipocyte hypertrophy. We note that the dWAT depot, alongside other fat depots, becomes depleted

when mice are given an extreme temperature challenge (transfer to 4°C)(40), which could compound their energetic stress.

For humans, this study has shown little correlation between SAF thickness and obesity, indeed the thickness of this layer is highly individual specific. The marginal increase in thickness between lean and overweight/obese individuals could be accounted for by the 20% increase in SAF adipocyte fat storage (**Table 1**). We speculate that both environmental and genetic factors may control the thickness, with impact for subsequent energy budget. Specific genes are known to regulate the pattern of human fat deposition, notably for example lower body subcutaneous depots (such as gluteofemoral) and peritoneal visceral fat (54, 55); there may be similar genes that regulate the thickness of SAF.

We also note that high variation in SAF volume may lead to a correspondingly high variation in the total heat generating capacity of this depot. Heat production in mammalian bodies is a zero-sum reaction, the demand for heat is fulfilled by various means, whether muscle exercise, activation of BAT, or activation of non-canonical futile cycles in beige fat, muscle or heart. This leads us to speculate that our observations could go some way to explaining the paradoxical differences observed for individual lean subjects in their capacity for BAT activation (56); BAT activation for any given individual may be inversely related to the total amount of skin-associated adipose tissue. It would also explain why obese subjects show little BAT activation, since these individuals typically have a large volume of subcutaneous fat pads.

We considered the possibility that the lipolytic hub, HSL, was not present to be activated in dWAT in response to β-adrenergic activation; however, activation of this enzyme has been observed during the lipid depletion associated with dWAT involution during catagen (57). The lack of HSL activation in dWAT stands in contrast to human SAF, where it is known that lipolysis is dependent upon HSL (58). Indeed, human scWAT has been shown to become lipolytic during the cool season (46, 59, 60), when mast cells are implicated as the lipolytic initiator. Indeed, only temporary but repeated application of an ice pack to thigh (30 minutes for 10 days) was enough to induce systemic activation of the β-adrenergic response. We would expect sustained lipolysis to deplete the SAF layer (Fig.7B); it remains to be tested whether intermittent cool exposure increases or

decreases the SAF layer or affects an individual's capacity for non-canonical heat generation by subcutaneous fat activation.

Mouse dWAT is highly dynamic compared to other fat depots (25), however, the time required for dWAT thickening in response to environmental cues is still on the order of days. We propose that dWAT thickening is a chronic adaptive response that mitigates heat loss when thermogenic demand is high. Acclimation to cold exposure reflects adaptive changes to heat production strategies; these are important, since they impact glucose homeostasis and insulin sensitivity (61-63). To narrow down the degree of exposure required to cue the thickening of dWAT in response to cooler environmental temperature, we exposed mice to room temperature for 12 hours out of each day, either during the waking period (night-time) or sleep period (daytime). Interestingly we found that the temperature of the mice during their sleep phase cued the development of thicker, cold-adapted dWAT, and we surmise that there is a component of circadian control of this process.

Note this cycling protocol was applied to singly housed mice; the typical sleeping temperature for group-housed mice is predicted to be warm, since mice build nests and huddle together to sleep. We conclude that our warm-sleep cycling protocol may be mimicked by group-housed mice. This implicates behavior as a regulator of dWAT thickness. The cycle of warm-sleep and cool-waking time was designed to mimic a typical human circadian environmental temperature exposure, with the goal of identifying whether there are dominant temperature exposures that train the thermogenic response of each individual mammal. Our data to date suggests that chronic adaptations are designed to minimize the total thermogenic load, therefore intermittent exposure to cool temperatures will likely have more benefit than longer chronic exposures, when homeostatic mechanisms are activated.

Scherer and colleagues defined aspects of mouse dermal adipocytes that make them unique, such as microenvironment, transcriptome and regulation. This group found that these adipocytes express distinguishing gene markers such as cathelicidin (CAMP1), collagen5 and CCL4 (40). We have shown that the most distinctive property of dWAT, that distinguishes it from its nearest neighbor, iWAT, is its ability to resist depletion in response to β-adrenergic activation (**Fig. 5; Table 1**).

Despite the distinct properties of human SAF and mouse dWAT, there is a functional similarity between the heat production strategies of mouse and human skin-associated depots. Thus, directly underneath the dWAT heat transfer barrier lie ten subcutaneous fat pads (mammary glands or male equivalent; **Fig. 8**) spread across the peritoneum, where the approximate surface area equals 10cm^2. These are highly responsive to β-adrenergic activation (including heterogeneous UCP1 induction), and we conclude that together, the dWAT and iWAT combination are functionally homologous to human skin-associated fat.

Methods

Mice. BALB/cJ (#00651), C57BL/6J (#00664), Agouti lethal yellow (A^y/a; C57BL/6J;#002468) and *UCP1-/-* C57BL/6J;#003124) mice were obtained from Jackson Labs and bred in-house. All animals were housed at constant temperature (19 -23^{0}C) in 12 h light/dark cycles with free access to water and standard chow (Harlan Teklad Global Diet 2020X). For high fat feeding, C57BL/6J mice were provided with Harlan Teklad diet#TD06415 (45% calories from fat); for calorie restriction (**CR**), *ad libitum* consumption rates of chow were measured for singly housed mice; mice were 25% calorie restricted using a 60% mix of AIN93M:40% CR (Bioserv cat#F05314) in control diet (AIN93M, Bioserv cat#F05312), pair-fed daily at 5 pm, for 5 weeks.

Histological Analysis. Skin, BAT, perigonadal WAT (vWAT) and mammary gland (iWAT) were dissected for histological processing as follows: Samples were paraformaldehyde-fixed (4%) overnight / 4°C and then paraffin-embedded for evaluation. Tissue sections were deparaffinized, re-hydrated and stained with either standard H&E or Trichrome protocols for visualization. For assay of dWAT thickness, 6 images of H&E-stained, non-anagen fields of skins (equivalent to ≥4500 μm linear dWAT) were assayed by image analysis (dividing total area by length). For immunofluorescent analysis, tissues were processed for heat-induced epitope retrieval, epitopes were blocked in 10% goat serum for 3 hours; samples were either incubated with Alexa-conjugated primary antibodies for 1 hour, or incubated overnight with the primary antibody, washed and incubated for 1h with secondary antibodies. Samples were visualized on a confocal microscope (Nikon A1RS Confocal Microscope). For fluorescent intensity assessment, at least 3 independent fields were obtained for each mouse sample, and signal was quantified using open source Fiji image processing package. In each case, the specific signal was normalized to the signal from lipid droplet–associated perilipin. For quantification of lipid droplet size, six independent fields were obtained and quantified using open source Fiji image processing package (https://loci.wisc.edu/software/fiji). Antibodies and immunohistochemical reagents were as follows: anti-CD31 (#3528), anti-CD31 (#77699), anti-Fabp4 (#3544), anti-Fatty acid synthase (FASN; #3180), anti-HSL (#4107), anti-pS565 HSL (#4137), anti-pS660 HSL (#4126), anti-pS 235/226 S6 (#2211, all Cell Signaling Technology); Alexa Fluor488 anti-perilipin (#NB110-40760AF488) and AlexaFluor647 anti-perilipin

(#NB110-40760AF647, both from Novus Biologicals); anti-UCP1 (#ab10983, Abcam); secondary reagents were AlexaFluor546 goat anti-rabbit (#A-11035), AlexaFluor546 goat anti-mouse (#A-11030) and AlexaFluor633 wheat germ agglutinin (#W21404) from Thermo Fisher Scientific.

3T3L1 cell culture. Mouse 3T3-L1 preadipocytes were from the American Tissue Culture Collection (ATCC) and were maintained in Dulbecco's modified Eagle's medium supplemented with 4.5 g/l of glucose (Life Technologies), 10% fetal bovine serum and 100-U/ml penicillin and streptomycin. Briefly, cells were differentiated into adipocytes using MDI medium (100 mg/ml 3-isobutyl-1-methylxanthine, 100 ng/ml dexamethasone and 1 mg/ml insulin, both from Sigma) for 4 days, followed by 1 mg/ml insulin for an additional 4 days (18), and fixed for immunofluorescent staining using 3% paraformaldehyde (20 mins/4°C).

β-adrenergic induction. The pan β-adrenergic agonist, isoproterenol hydrochloride (**ISO**) was from Sigma; the β3-adrenoreceptor agonists, CL 316,243 disodium salt (**CL**) was obtained from Tocris Bioscience (UK) and mirabegron (**Mira**) was from Cayman Chemical. For CL administration *in vivo*, mice were acclimated to thermoneutrality for 3 days, injected with 1 mg/kg CL, and euthanized for tissue collection 60 minutes later. For β-adrenergic stimulation *in vitro*, 3T3-L1 cells were treated with ISO (10 μM) for 40 minutes at 37°C. For β-adrenergic stimulation *ex vivo*, human fat samples (approx. 0.5cm in size) were treated with ISO (10 μM) for 40 minutes at 37°C. For β-adrenergic stimulation *in vivo*, human subjects were administered Mira for 10 weeks (50 mg/day), with abdominal adipose biopsies before and after treatment, as described previously (46).

FLIR imaging. To measure surface temperatures by infrared thermography, we used a hand-held FLIR T360 camera (FLIR Systems, Oregon). Pin drops in the software of the FLIR camera were used to record surface temperatures and quantified using FLIR Tools Advanced Thermal Analysis and Reporting software; each photograph is internally and externally calibrated to show actual temperatures (31).

SHIP study design and acquisition of MRI images of skin-associated fat. The Study of Health in Pomerania (SHIP) study is a longitudinal study of health parameters for over 4000 adults (20-79), representative of an area with population >200 000 (64). The assay of the thickness of skin-associated fat (SAF) was performed using a chemical shift-encoded 3D gradient-echo sequence of the whole-body (1.5T MR

images, Avanto, Siemens Healthcare), with the following parameters: repetition time = 12 ms, echo time (s) = 2.38 ms, flip angle = 5°, spatial resolution 1.95 mm x 1.95 mm x 5 mm, acquisition matrix 0/256/128/0, pixel bandwidth 1955 Hz/Pixel of each series with complete imaging of both calves. MR sequences were postprocessed to separate confounder corrected water- and fat-only images. Confounder-corrected fat only images were used to measure skin-associated fat (65). Skin associated fat was measured at the lateral side of both legs, 30% distance between tibia and ankle diaphysis.

Collection of human samples. Breast tissues were collected during breast reduction surgeries by the University of Wisconsin Carbone Cancer center Translational Science Biocore Biobank. Human skin samples (with associated fat) were obtained from patients undergoing elective reconstructive surgeries at our institution. The de-identified samples were exempt from the regulation of University of Wisconsin-Madison Human Subjects Committee Institutional Review Boards. Data on patient age, sex, and type of surgery were collected with the tissues. Skin samples were processed within 3 hours of surgery.

Statistics. Statistical tests were selected from unpaired two tailed *t* tests, ordinary one-way ANOVA with Tukey's multiple comparisons test or with Kruskal-Wallis test (with Dunn's multiple comparisons) as indicated in Figure legends. Analyses were conducted using GraphPrism8 software; outliers were identified using ROUT method; data are expressed as mean ± SEM unless otherwise stated. The type of correlation analysis is indicated in the Figure legends. To test for normal or lognormal distribution of sample values we used the Anderson-Darling test. Box-and-whiskers graphs show median values with 5-95 percentile whiskers.

Study Approval: Mice. These studies were performed in strict accordance with the recommendations in the Guide for the Care and Use of Laboratory Animals of the National Institutes of Health. Experimental protocols were approved by the University of Wisconsin School of Medicine and Public Health Animal Care and Use Committee. The number of mice used to perform this study was minimized, and every effort was made to reduce the chance of pain or suffering.

Human Subjects. Subjects were consented for the SHIP study as part of the Community Medicine Research Net of the University of Greifswald, Germany; the University of Greifswald is a member of the 'Center of

Knowledge Interchange' program of Siemens AG. All analysis of SHIP data that included the use of human subjects was HIPAA-compliant and was performed after obtaining approval from the University of Wisconsin Institutional Review Board. At the University of Wisconsin, human skin specimens were taken from discarded tissues during defect reconstruction and body sculpting procedures, and were used for research, anonymously, under IRB approvals (University of Wisconsin Skin Disease Research Center and Biocore Biobank).

Author contributions

CMA Development of strategy, execution of experimental procedures, consultation with analysis, manuscript preparation; **IK** Design and execution of experimental procedures, data analysis and presentation, manuscript preparation**; JK, HZ, RB, DH** Design and execution of MRI imaging procedures, data analysis and presentation**; AG, YZ, JS, PK** Collection of human skin and fat samples; **CLEY, DN, NR, DL** Development of strategy, consultation on mouse metabolic studies, supply of samples from mice on high fat feeding protocols**; OM** Development of strategy, manuscript preparation

Acknowledgements. This work was supported by RO1GM113142 (CMA, IK); a pilot award from the University of Wisconsin Skin Disease Research Center (SDRC) NIAMS P30 AR066524 (IK); the University of Wisconsin Carbone Comprehensive Cancer Center (UWCCC) for use of its Shared Services (NIH/NCI P30 CA014520), including the Translational Initiatives in Pathology (TrIP) lab and Translational Science Biocore (TSB); R01 DK112282 and UL1 TR001998 (PK); R24DK092759, R01DK121759 and R01DK125513 (OAM), UW Institute on Aging, NIA T32 AG000213 (NER), NIH/National Institute on Aging, AG056771, AG062328, and AG061635 (DWL), the U.S. Department of Veterans Affairs, I01-BX004031 (DWL) and the facilities and resources from the William S. Middleton Memorial Veterans Hospital. SHIP is part of the Community Medicine Research Net of the University of Greifswald, Germany, which is funded by the Federal Ministry of Education and Research (01ZZ9603, 01ZZ0103, 01ZZ0403, 01ZZ0701, 03ZIK012), the Ministry of Cultural

Affairs as well as the Social Ministry of the Federal State of Mecklenburg-West Pomerania. Whole-body MR imaging was supported by a joint grant from Siemens Healthcare, Erlangen, Germany, and the Federal State of Mecklenburg-West Pomerania. We appreciate expert technical assistance from Edgar Ocotl, the University of Wisconsin Translational Research Initiatives in Pathology laboratory (TRIP), and the Biobank, supported by the UW Department of Pathology and Laboratory Medicine, UWCCC (P30 CA014520) and the Office of The Director- NIH (S10OD023526). We acknowledge the donation of Sprague-Dawley rat skins from Dr. Kumar (Department of Comparative Biosciences, UW).

References

1. Lee MJ, Wu Y, and Fried SK. Adipose tissue heterogeneity: implication of depot differences in adipose tissue for obesity complications. *Mol Aspects Med*. 2013;34(1):1-11.
2. Pinnick KE, Nicholson G, Manolopoulos KN, McQuaid SE, Valet P, Frayn KN, et al. Distinct developmental profile of lower-body adipose tissue defines resistance against obesity-associated metabolic complications. *Diabetes*. 2014;63(11):3785-97.
3. Manolopoulos KN, Karpe F, and Frayn KN. Gluteofemoral body fat as a determinant of metabolic health. *Int J Obes (Lond)*. 2010;34(6):949-59.
4. Karastergiou K, and Fried SK. Multiple adipose depots increase cardiovascular risk via local and systemic effects. *Curr Atheroscler Rep*. 2013;15(10):361.
5. Walker GE, Marzullo P, Ricotti R, Bona G, and Prodam F. The pathophysiology of abdominal adipose tissue depots in health and disease. *Horm Mol Biol Clin Investig*. 2014;19(1):57-74.
6. Yoneshiro T, Aita S, Matsushita M, Kayahara T, Kameya T, Kawai Y, et al. Recruited brown adipose tissue as an antiobesity agent in humans. *J Clin Invest*. 2013;123(8):3404-8.
7. Smith GI, Mittendorfer B, and Klein S. Metabolically healthy obesity: facts and fantasies. *J Clin Invest*. 2019;129(10):3978-89.
8. Karastergiou K, Smith SR, Greenberg AS, and Fried SK. Sex differences in human adipose tissues - the biology of pear shape. *Biol Sex Differ*. 2012;3(1):13.
9. Kasza I, Hernando D, Roldan-Alzate A, Alexander CM, and Reeder SB. Thermogenic profiling using magnetic resonance imaging of dermal and other adipose tissues. *JCI Insight*. 2016;1(13):e87146.
10. Nicu C, Pople J, Bonsell L, Bhogal R, Ansell DM, and Paus R. A guide to studying human dermal adipocytes in situ. *Exp Dermatol*. 2018;27(6):589-602.
11. Driskell RR, Jahoda CA, Chuong CM, Watt FM, and Horsley V. Defining dermal adipose tissue. *Exp Dermatol*. 2014;23(9):629-31.
12. Kruglikov IL, and Scherer PE. Dermal Adipocytes: From Irrelevance to Metabolic Targets? *Trends Endocrinol Metab*. 2016;27(1):1-10.

13. Zwick RK, Guerrero-Juarez CF, Horsley V, and Plikus MV. Anatomical, Physiological, and Functional Diversity of Adipose Tissue. *Cell Metab*. 2018;27(1):68-83.

14. Kelley DE, Thaete FL, Troost F, Huwe T, and Goodpaster BH. Subdivisions of subcutaneous abdominal adipose tissue and insulin resistance. *American journal of physiology Endocrinology and metabolism*. 2000;278(5):E941-8.

15. Karastergiou K, and Fried SK. Cellular Mechanisms Driving Sex Differences in Adipose Tissue Biology and Body Shape in Humans and Mouse Models. *Adv Exp Med Biol*. 2017;1043:29-51.

16. Wajchenberg BL. Subcutaneous and visceral adipose tissue: their relation to the metabolic syndrome. *Endocr Rev*. 2000;21(6):697-738.

17. Smith SR, Lovejoy JC, Greenway F, Ryan D, deJonge L, de la Bretonne J, et al. Contributions of total body fat, abdominal subcutaneous adipose tissue compartments, and visceral adipose tissue to the metabolic complications of obesity. *Metabolism*. 2001;50(4):425-35.

18. Kasza I, Suh Y, Wollny D, Clark RJ, Roopra A, Colman RJ, et al. Syndecan-1 is required to maintain intradermal fat and prevent cold stress. *PLoS Genet*. 2014;10(8):e1004514.

19. Speakman JR. Measuring energy metabolism in the mouse - theoretical, practical, and analytical considerations. *Front Physiol*. 2013;4:34.

20. Tschop MH, Speakman JR, Arch JR, Auwerx J, Bruning JC, Chan L, et al. A guide to analysis of mouse energy metabolism. *Nature methods*. 2012;9(1):57-63.

21. Elattar S, and Satyanarayana A. Can Brown Fat Win the Battle Against White Fat? *J Cell Physiol*. 2015;230(10):2311-7.

22. Cannon B, and Nedergaard J. Thermogenesis challenges the adipostat hypothesis for body-weight control. *Proc Nutr Soc*. 2009;68(4):401-7.

23. Harms M, and Seale P. Brown and beige fat: development, function and therapeutic potential. *Nature medicine*. 2013;19(10):1252-63.

24. Bartelt A, and Heeren J. Adipose tissue browning and metabolic health. *Nat Rev Endocrinol*. 2014;10(1):24-36.

25. Alexander CM, Kasza I, Yen CL, Reeder SB, Hernando D, Gallo RL, et al. Dermal white adipose tissue: a new component of the thermogenic response. *J Lipid Res*. 2015;56(11):2061-9.

26. Neess D, Bek S, Bloksgaard M, Marcher AB, Faergeman NJ, and Mandrup S. Delayed hepatic adaptation to weaning in ACBP-/- mice is caused by disruption of the epidermal barrier. *Cell Rep*. 2013;5(5):1403-12.

27. Kruse V, Neess D, and Faergeman NJ. The Significance of Epidermal Lipid Metabolism in Whole-Body Physiology. *Trends Endocrinol Metab*. 2017;28(9):669-83.

28. Shih MY, Kane MA, Zhou P, Yen CL, Streeper RS, Napoli JL, et al. Retinol Esterification by DGAT1 Is Essential for Retinoid Homeostasis in Murine Skin. *J Biol Chem*. 2009;284(7):4292-9.

29. Sampath H, Flowers MT, Liu X, Paton CM, Sullivan R, Chu K, et al. Skin-specific deletion of stearoyl-CoA desaturase-1 alters skin lipid composition and protects mice from high fat diet-induced obesity. *The Journal of biological chemistry*. 2009;284(30):19961-73.

30. Sampath H, and Ntambi JM. Role of stearoyl-CoA desaturase-1 in skin integrity and whole body energy balance. *J Biol Chem*. 2014;289(5):2482-8.

31. Kasza I, Adler D, Nelson DW, Eric Yen CL, Dumas S, Ntambi JM, et al. Evaporative cooling provides a major metabolic energy sink. *Mol Metab*. 2019;27:47-61.

32. Grove KL, Fried SK, Greenberg AS, Xiao XQ, and Clegg DJ. A microarray analysis of sexual dimorphism of adipose tissues in high-fat-diet-induced obese mice. *Int J Obes (Lond)*. 2010;34(6):989-1000.

33. Kruglikov IL, and Scherer PE. Dermal adipocytes and hair cycling: is spatial heterogeneity a characteristic feature of the dermal adipose tissue depot? *Exp Dermatol*. 2016;25(4):258-62.

34. Sbarbati A, Accorsi D, Benati D, Marchetti L, Orsini G, Rigotti G, et al. Subcutaneous adipose tissue classification. *Eur J Histochem*. 2010;54(4):e48.

35. Cappellano G, Morandi EM, Rainer J, Grubwieser P, Heinz K, Wolfram D, et al. Human Macrophages Preferentially Infiltrate the Superficial Adipose Tissue. *Int J Mol Sci*. 2018;19(5).

36. Enevoldsen LH, Simonsen L, Stallknecht B, Galbo H, and Bulow J. In vivo human lipolytic activity in preperitoneal and subdivisions of subcutaneous abdominal adipose tissue. *Am J Physiol Endocrinol Metab*. 2001;281(5):E1110-4.

37. Wu J, Bostrom P, Sparks LM, Ye L, Choi JH, Giang AH, et al. Beige adipocytes are a distinct type of thermogenic fat cell in mouse and human. *Cell*. 2012;150(2):366-76.

38. Mottillo EP, Balasubramanian P, Lee YH, Weng C, Kershaw EE, and Granneman JG. Coupling of lipolysis and de novo lipogenesis in brown, beige, and white adipose tissues during chronic beta3-adrenergic receptor activation. *J Lipid Res*. 2014;55(11):2276-86.

39. Chondronikola M, and Sidossis LS. Brown and beige fat: From molecules to physiology. *Biochim Biophys Acta Mol Cell Biol Lipids*. 2019;1864(1):91-103.

40. Zhang Z, Shao M, Hepler C, Zi Z, Zhao S, An YA, et al. Dermal adipose tissue has high plasticity and undergoes reversible dedifferentiation in mice. *J Clin Invest*. 2019;129(12):5327-42.

41. Ogasawara J, Izawa T, Sakurai T, Sakurai T, Shirato K, Ishibashi Y, et al. The Molecular Mechanism Underlying Continuous Exercise Training-Induced Adaptive Changes of Lipolysis in White Adipose Cells. *J Obes*. 2015;2015:473430.

42. Fruhbeck G, Mendez-Gimenez L, Fernandez-Formoso JA, Fernandez S, and Rodriguez A. Regulation of adipocyte lipolysis. *Nutr Res Rev*. 2014;27(1):63-93.

43. Liu D, Bordicchia M, Zhang C, Fang H, Wei W, Li JL, et al. Activation of mTORC1 is essential for beta-adrenergic stimulation of adipose browning. *J Clin Invest*. 2016;126(5):1704-16.

44. Scheller EL, Khandaker S, Learman BS, Cawthorn WP, Anderson LM, Pham HA, et al. Bone marrow adipocytes resist lipolysis and remodeling in response to beta-adrenergic stimulation. *Bone*. 2019;118:32-41.

45. Keipert S, Lutter D, Schroeder BO, Brandt D, Stahlman M, Schwarzmayr T, et al. Endogenous FGF21-signaling controls paradoxical obesity resistance of UCP1-deficient mice. *Nat Commun*. 2020;11(1):624.

46. Finlin BS, Memetimin H, Confides AL, Kasza I, Zhu B, Vekaria HJ, et al. Human adipose beiging in response to cold and mirabegron. *JCI Insight*. 2018;3(15).

47. Chouchani ET, Kazak L, and Spiegelman BM. New Advances in Adaptive Thermogenesis: UCP1 and Beyond. *Cell Metab*. 2019;29(1):27-37.

48. Chen KY, Cypess AM, Laughlin MR, Haft CR, Hu HH, Bredella MA, et al. Brown Adipose Reporting Criteria in Imaging STudies (BARCIST 1.0): Recommendations for Standardized FDG-PET/CT Experiments in Humans. *Cell Metab*. 2016;24(2):210-22.

49. Mills EL, Pierce KA, Jedrychowski MP, Garrity R, Winther S, Vidoni S, et al. Accumulation of succinate controls activation of adipose tissue thermogenesis. *Nature*. 2018;560(7716):102-6.

50. Kazak L, Rahbani JF, Samborska B, Lu GZ, Jedrychowski MP, Lajoie M, et al. Ablation of adipocyte creatine transport impairs thermogenesis and causes diet-induced obesity. *Nat Metab*. 2019;1(3):360-70.

51. Ikeda K, Kang Q, Yoneshiro T, Camporez JP, Maki H, Homma M, et al. UCP1-independent signaling involving SERCA2b-mediated calcium cycling regulates beige fat thermogenesis and systemic glucose homeostasis. *Nat Med*. 2017;23(12):1454-65.

52. Fabbiano S, Suarez-Zamorano N, Rigo D, Veyrat-Durebex C, Stevanovic Dokic A, Colin DJ, et al. Caloric Restriction Leads to Browning of White Adipose Tissue through Type 2 Immune Signaling. *Cell Metab*. 2016;24(3):434-46.

53. Kajimura S, Spiegelman BM, and Seale P. Brown and Beige Fat: Physiological Roles beyond Heat Generation. *Cell Metab*. 2015;22(4):546-59.

54. Lu Y, Day FR, Gustafsson S, Buchkovich ML, Na J, Bataille V, et al. New loci for body fat percentage reveal link between adiposity and cardiometabolic disease risk. *Nat Commun*. 2016;7:10495.

55. Loh NY, Neville MJ, Marinou K, Hardcastle SA, Fielding BA, Duncan EL, et al. LRP5 Regulates Human Body Fat Distribution by Modulating Adipose Progenitor Biology in a Dose- and Depot-Specific Fashion. *Cell metabolism*. 2015;21(2):262-72.

56. van Marken Lichtenbelt WD, Vanhommerig JW, Smulders NM, Drossaerts JM, Kemerink GJ, Bouvy ND, et al. Cold-activated brown adipose tissue in healthy men. *The New England journal of medicine*. 2009;360(15):1500-8.

57. Rivera-Gonzalez GC, Shook BA, Andrae J, Holtrup B, Bollag K, Betsholtz C, et al. Skin Adipocyte Stem Cell Self-Renewal Is Regulated by a PDGFA/AKT-Signaling Axis. *Cell Stem Cell*. 2016;19(6):738-51.

58. Langin D, Dicker A, Tavernier G, Hoffstedt J, Mairal A, Ryden M, et al. Adipocyte lipases and defect of lipolysis in human obesity. *Diabetes*. 2005;54(11):3190-7.

59. Kern PA, Finlin BS, Zhu B, Rasouli N, McGehee RE, Jr., Westgate PM, et al. The effects of temperature and seasons on subcutaneous white adipose tissue in humans: evidence for thermogenic gene induction. *J Clin Endocrinol Metab*. 2014;99(12):E2772-9.

60. Finlin BS, Zhu B, Confides AL, Westgate PM, Harfmann BD, Dupont-Versteegden EE, et al. Mast Cells Promote Seasonal White Adipose Beiging in Humans. *Diabetes*. 2017;66(5):1237-46.

61. Hanssen MJ, van der Lans AA, Brans B, Hoeks J, Jardon KM, Schaart G, et al. Short-term Cold Acclimation Recruits Brown Adipose Tissue in Obese Humans. *Diabetes*. 2016;65(5):1179-89.

62. van der Lans AA, Hoeks J, Brans B, Vijgen GH, Visser MG, Vosselman MJ, et al. Cold acclimation recruits human brown fat and increases nonshivering thermogenesis. *J Clin Invest*. 2013;123(8):3395-403.

63. Yoneshiro T, Matsushita M, Nakae S, Kameya T, Sugie H, Tanaka S, et al. Brown adipose tissue is involved in the seasonal variation of cold-induced thermogenesis in humans. *Am J Physiol Regul Integr Comp Physiol*. 2016:ajpregu 00057 2015.

64. Volzke H, Alte D, Schmidt CO, Radke D, Lorbeer R, Friedrich N, et al. Cohort profile: the study of health in Pomerania. *Int J Epidemiol*. 2011;40(2):294-307.

65. Kuhn JP, Meffert P, Heske C, Kromrey ML, Schmidt CO, Mensel B, et al. Prevalence of Fatty Liver Disease and Hepatic Iron Overload in a Northeastern German Population by Using Quantitative MR Imaging. *Radiology*. 2017;284(3):706-16.

Table 1. Summary comparison of key features of skin-associated fat depots for mouse and human.

Parameter	Mouse dWAT	Human SAF	comments
Morphology	Segregated from nearest adjacent scWAT depots by muscle layer	Not partitioned by muscle: partitioned instead into collagen-wrapped "bubble wrap"	(25) (11) (12)
Thickness	0-400 μm Varies depending upon age, sex, strain, adiposity	3-15 mm Highly variable from subject to subject	(Dimension quoted for lean subjects)
Size of adipocytes (diameter)	40 ± 1.7 μm / lean mice 59 ± 5.5 μm / obese mice ≈50% increase Adipocytes from iWAT and dWAT are similar size, and half the size of vWAT adipocytes.	56 ± 1.1 μm /lean subjects 67 ± 0.7 μm /obese subjects ≈20% increase Subcutaneous and visceral adipocytes are similar sizes	Combined data from human, for several body sites (breast, abdominal, visceral, thigh; lean, n=7, obese n=8) and for mice, either genetically obese (A^y) or fed high fat diet (n=9, obese; n=26, lean).
Reaction to obesity	Thickens; size of adipocytes increases. Resistant to macrophage infiltration (crown-like structures)	No change of thickness in men; marginal change in women (<10%) Susceptible to macrophage infiltration (35)	Size of human abdominal scWAT adipocytes increases in obese subjects (66, 67) High fat diet feeding leads to expansion of mouse dWAT adipocytes (9, 40)
Reaction to calorie restriction	Becomes depleted in parallel with other adipose depots (in C57BL/6J males), although approx. half of dWAT is protected.	Not known. However, lean and obese men show the same thickness of SAF	Little association of low or high body-wide adiposity with SAF thickness in humans

Rate of accumulation and involution	Highly dynamic in response to hair growth, skin infection, environmental temperature	Unknown	(13, 25)
Male/female dimorphism	Thicker in females than males for BALB/cJ mice, but not C57BL/6J mice	Thicker in females than males	
Age-dependent maturation	Thickness increases steeply from 20-300 μm from 20-30 weeks of age for C57BL/6J males prior to, and during, a phase of rapid weight gain. Other mice do not show this regulation.	No change of thickness for SHIP study subjects (both male and female), between ages 20-79.	
Molecular reaction to β-adrenergic stimulants	No significant reaction of lipolytic hub enzyme (activating pS^{S660} HSL and inhibitory pS^{565} HSL), or mTOR activation ($pS^{235/236}$ S6); no significant lipid depletion assayed from lipid droplet size.	Majority of skin-associated adipocytes (scWAT fat pads or SAF) react (including HSL and S6 activation), and become lipid depleted, measured from adipocyte size after *ex vivo* stimulation.	HSL activation corresponds to active lipolysis, assayed by adipocyte shrinkage Little functional heterogeneity of human depots
Functional reaction to cooling	Thickens in response to activated thermogenesis (room temperature housing), and in mice with highly induced non-canonical thermogenic processes (UCP1KO). Accumulation depends upon timing of cool exposure	Lipolysis is activated in majority of skin-associated adipocytes, and SAF is therefore predicted to become depleted. Thermogenic activation of scWAT directly induces heat production	Skin-associated adipocytes of human and mouse have opposite responses to sub-thermoneutral environments: mouse dWAT increases to oppose heat loss; human SAF becomes lipolytic and actively participates in heat generation

Fig. 1

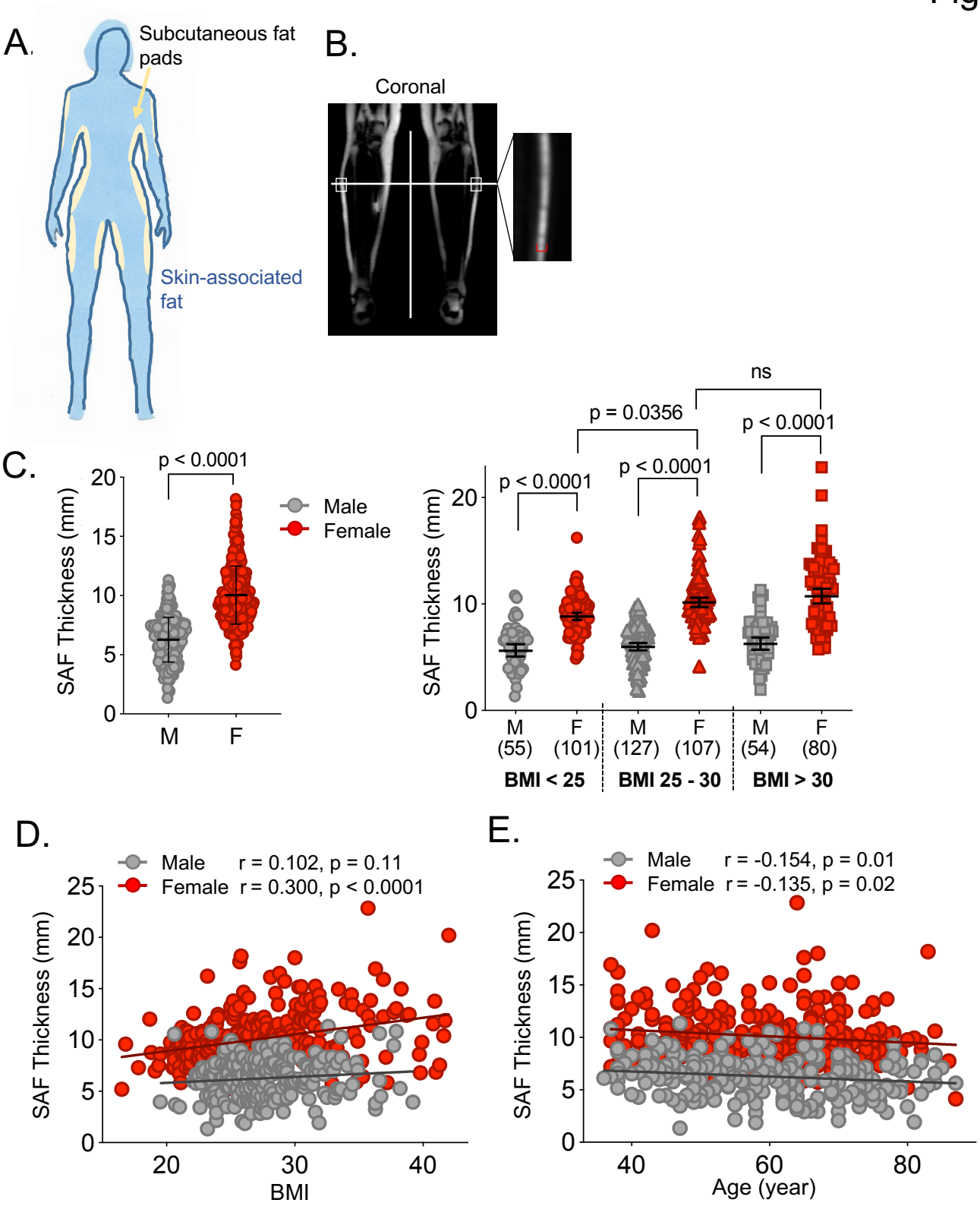

Fig. 1. The thickness of skin-associated fat is highly variable between human subjects, and independent of BMI. **A.** Cartoon illustrates the use of assay terminology. Ectopic subcutaneous fat pads are colored yellow; the body wide depot of skin associated fat colored dark blue. **B.** Assay of skin associated fat measured using coronal, fat-only MRI views of lower leg, 30% of distance between knee and ankle. A comparison of the standard fat/water composite image with the fat-only image is shown on the right-hand side. **C**. Results of SAF thickness assay for men (n=236) and women (n=286); these data were divided into groups, lean (BMI<25), overweight (BMI 25-30) and obese (BMI>30), with the indicated n numbers. Data are represented as geometric mean with 95% confidence interval. Distribution were tested by Anderson-Darling test. The data were analyzed by Kruskal-Wallis nonparametric test using Dunn's multiple comparisons test. **D,E.** Evaluation of correlation between BMI, age and SAF thickness, for men and women.

Fig. 2

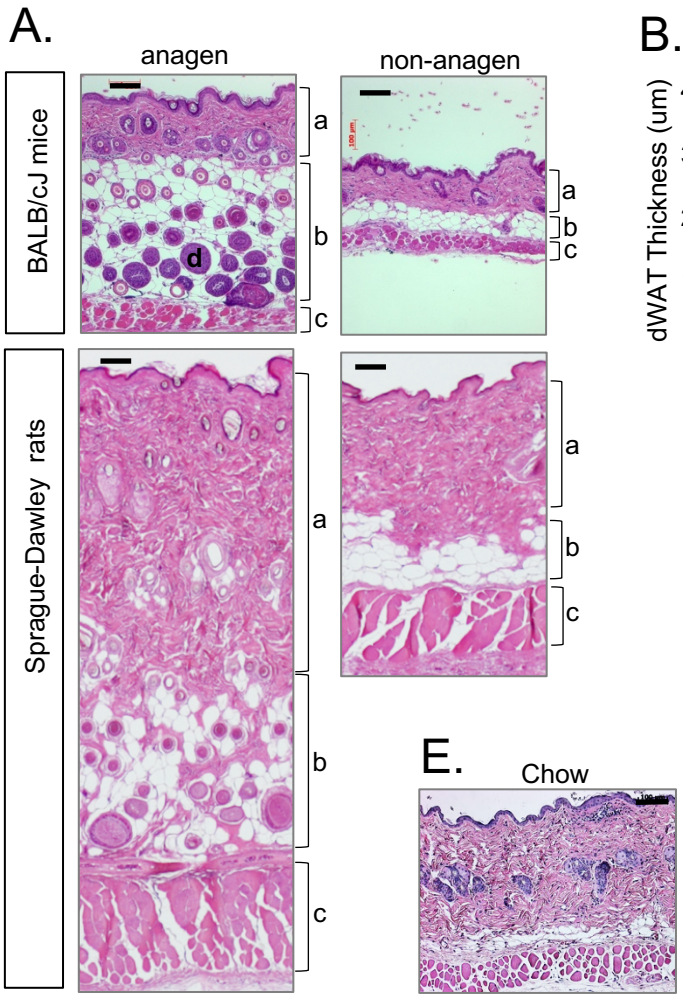

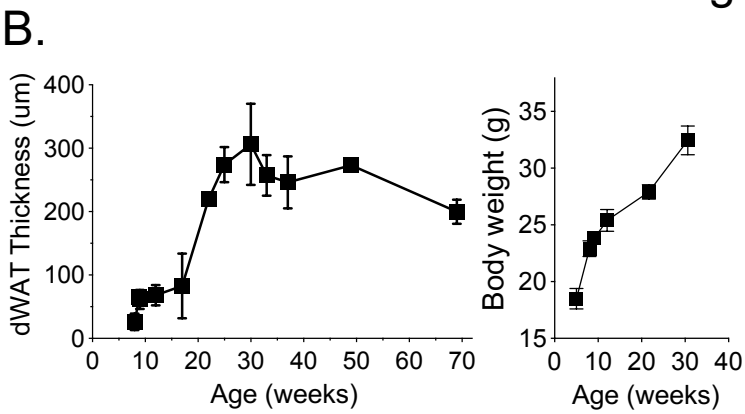

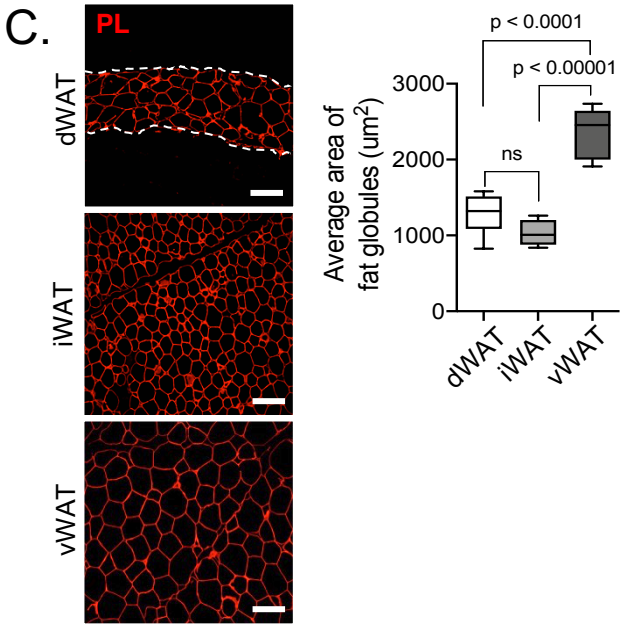

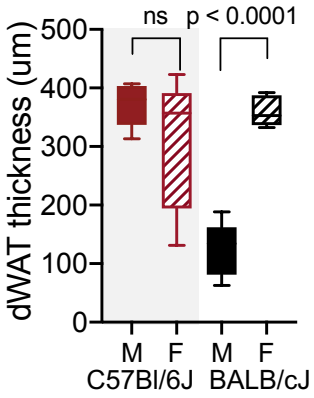

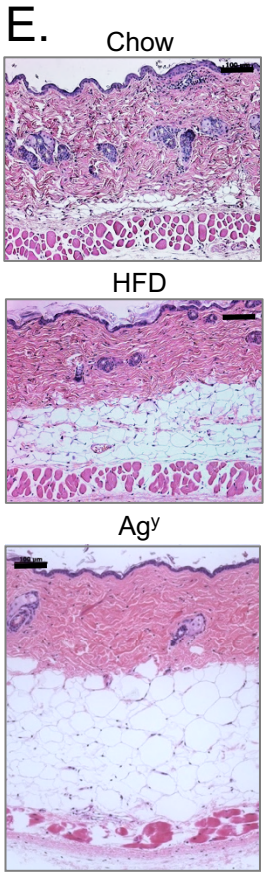

Fig. 2. Determinants of rodent dWAT thickness; age, sex, hair cycle, and obesity. A. *Hair cycle associated expansion*. Representative H&E stained sections of skin of rats and mice in non-anagen and anagen (follicular development) phases. **a**, dermis/epidermis; **b**, dWAT; **c,** *panniculus carnosus*; **d**, hair follicle. Scale bars=100 μm. **B.** *Maturation dependent accumulation*. Assay of dWAT thickness during the maturation of male C57BL/6J mice; n=65 mice. **C.** *Dermal adipocytes match inguinal adipocyte size.* Comparison of the sizes of fat globules in dermal (dWAT), inguinal (subcutaneous; iWAT) and visceral (vWAT) adipocytes from lean mice, as measured by immunofluorescent visualization using anti-perilipin (PL); n=6. Scale bars=100 μm. **D.** *Thickness of dWAT is highly sex- and strain-dependent.* dWAT thickness was measured from H&E sections of skins from C57Bl/J or BALB/cJ male and female mice >30 weeks old (n=6). Data of panels B and D were analyzed by unpaired two tailed *t* test; groups compared for panel C were analyzed by one-way ANOVA followed by Tukey's multiple comparisons test. **E.** *Number and size of dermal adipocytes increases in obese mice*. Representative H&E sections of dorsal skins from C57BL/6J male mice (7-11 weeks; n=6), fed chow or high fat diet for 5 weeks, or from a genetically obese model (1 year old C57BL/6J-Ag^{y} ; n=3). Average diameters are shown in Table 1. Scale bars=100 μm.

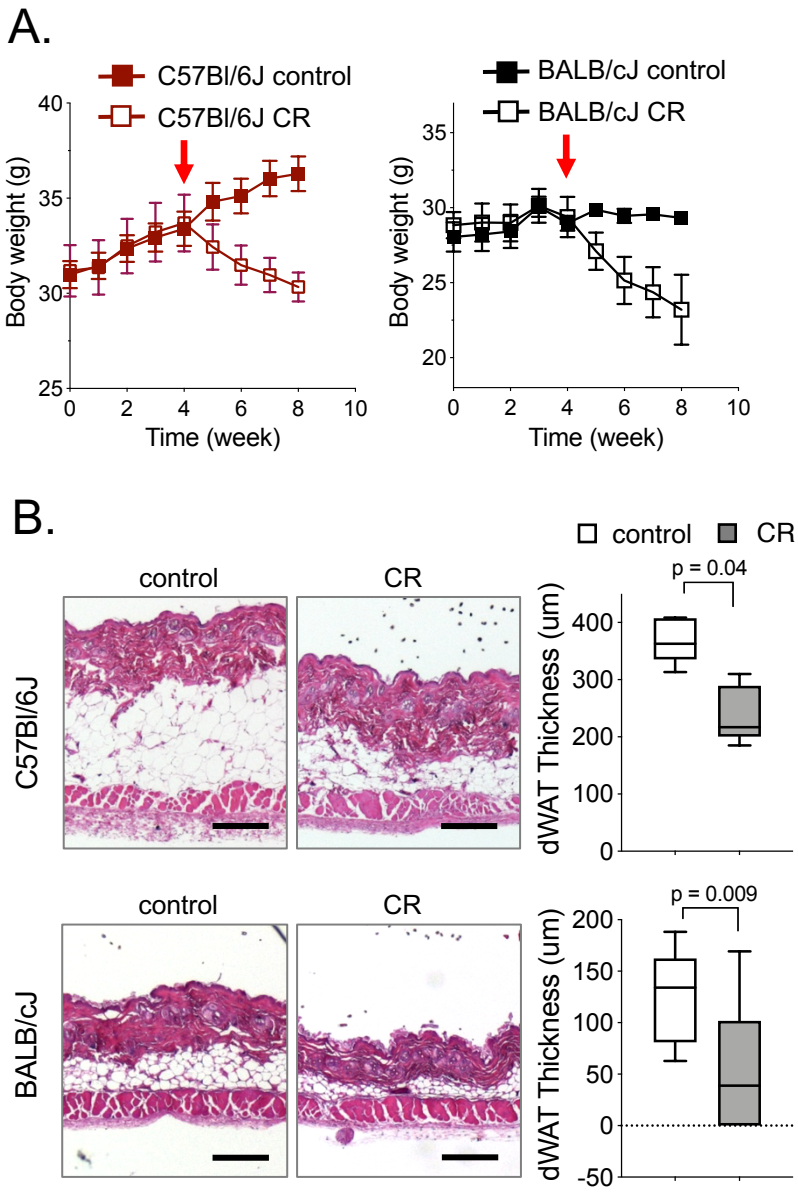

Fig. 3. **Calorie restriction depletes dWAT. A.** Body weight changes for C57BL/6J or BALB/cJ male mice (28 to 30-week-old) after 25% calorie restriction for 4 weeks (red arrow indicates start of dietary regime); n=6. **B.** dWAT thickness was assessed from H&E sections of dorsal skin. Scale bars=300 μm. Data were analyzed by unpaired two tailed *t* test.

Fig. 4

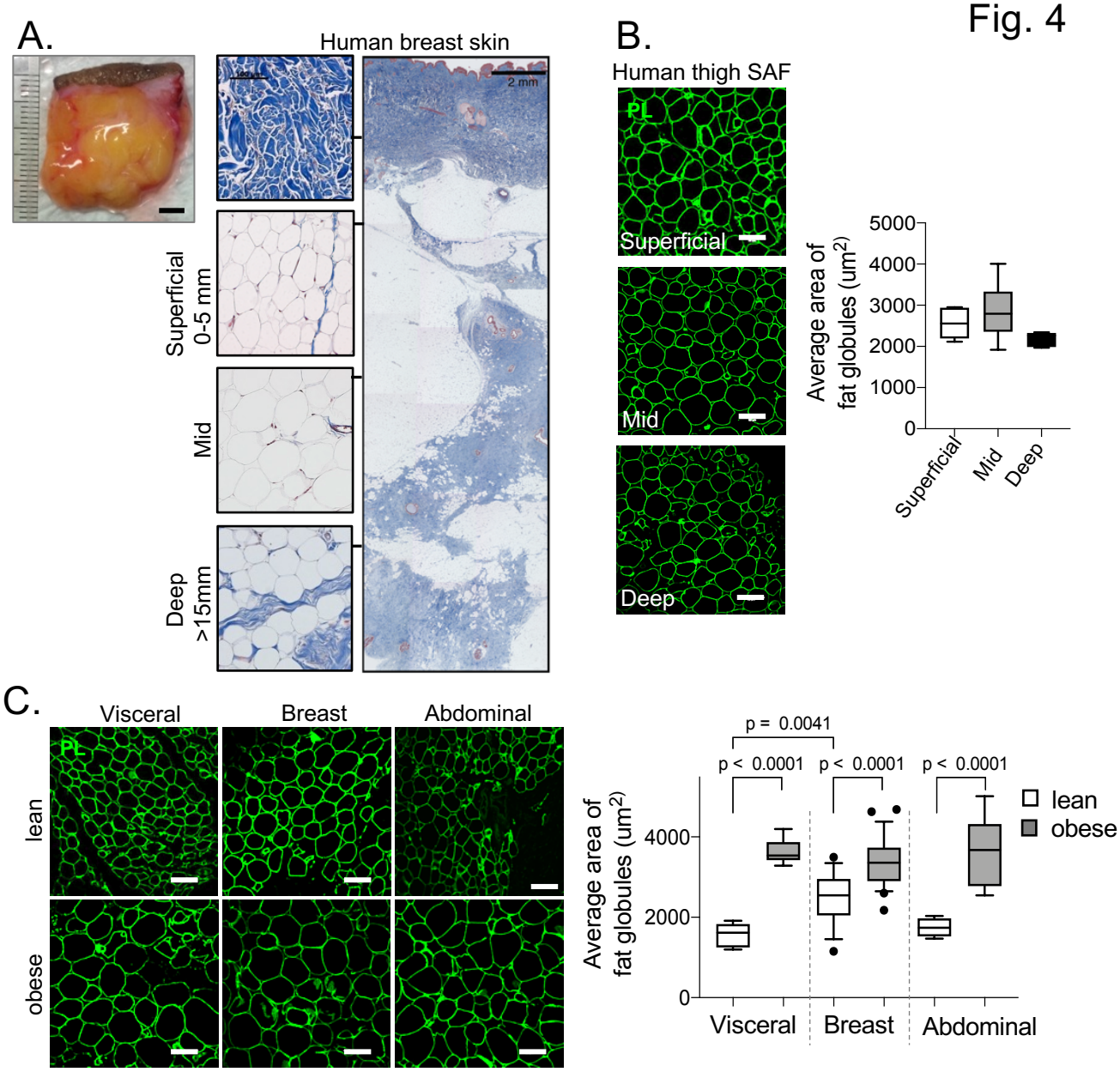

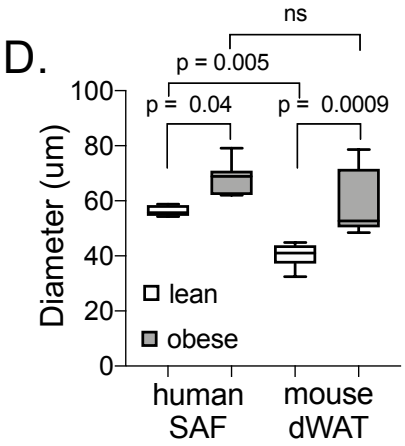

Fig. 4. Like mouse dermal adipocytes, human skin-associated adipocytes hypertrophy in obese subjects. **A.** Gross view and trichrome-stained sections of SAF from breast of a lean subject, with detail insets shown for dermis, superficial, mid and deep layers of adipocytes. Scale bars=5 mm on gross view, 2 mm on Trichrome-stained low power view, and 100 μm on high power detail insets. **B.** Human thigh tissue sections were stained with perilipin antibody (n=3); representative images are shown, with quantitation of the size of adipocytes from superficial, mid and deep layers. Scale bars=100 μm. **C.** *Comparison of SAF from breast and abdomen with visceral WAT*. Representative images of PLIN-stained fat globules from lean and obese subjects (left) were quantified (right); scale bars=100 μm. Data were analyzed by one-way ANOVA followed by Tukey's multiple comparisons test. **D.** *Adipocytes of mouse dWAT and human SAF respond similarly to obesogenesis.* The relative size of adipocytes in human SAF and mouse dWAT are shown for lean and obese subjects (human lean, n=5; human obese, n=7; mouse lean, n=7; mouse obese, n=5). Data were analyzed using a one-way ANOVA followed by Tukey's multiple comparisons test.

Fig. 5

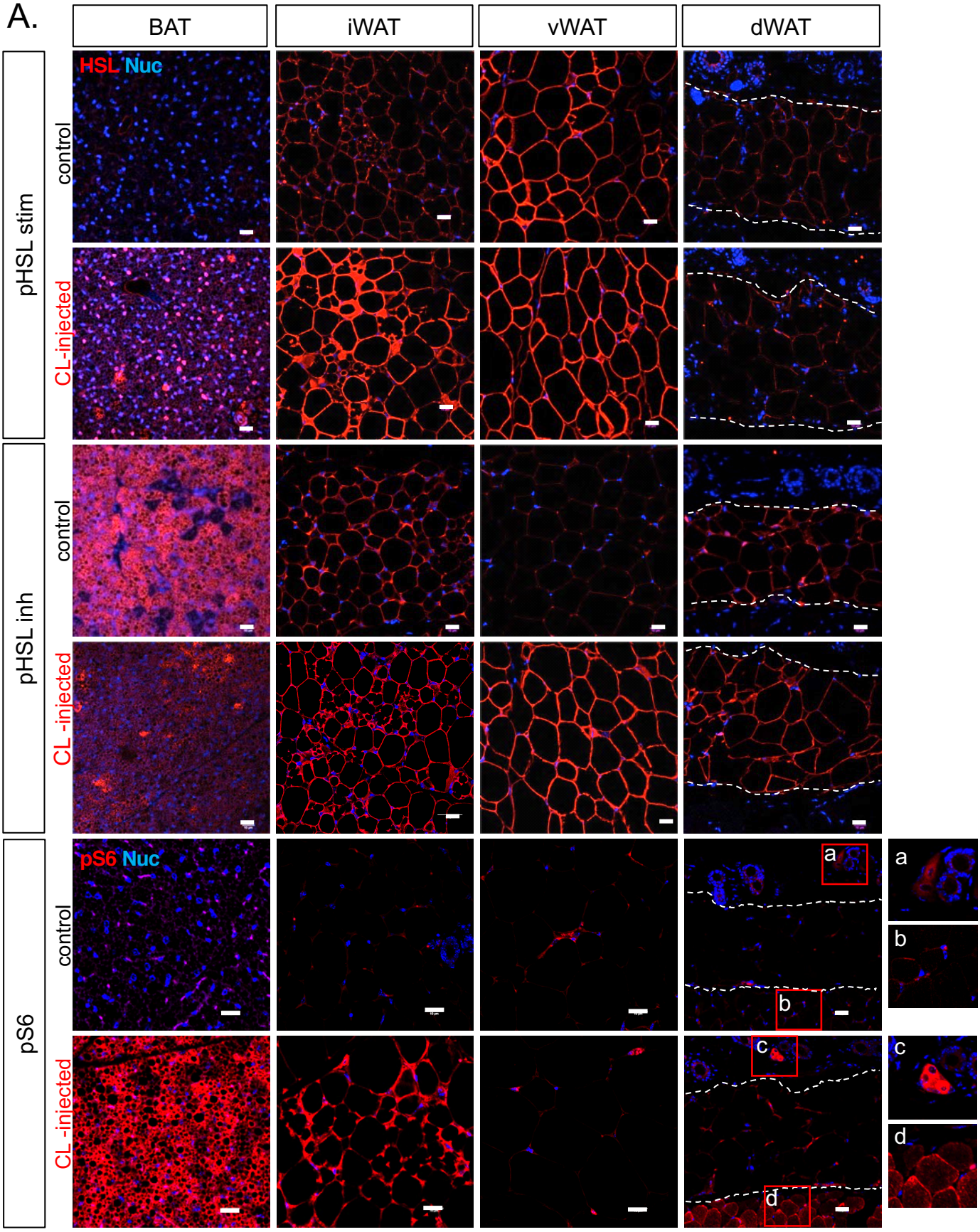
A.
BAT
iWAT
vWAT
dWAT
pHSL stim
control
CL-injected
HSL Nuc
pHSL inh
control
CL -injected
pS6
control
CL -injected
pS6 Nuc
a
b
c
d

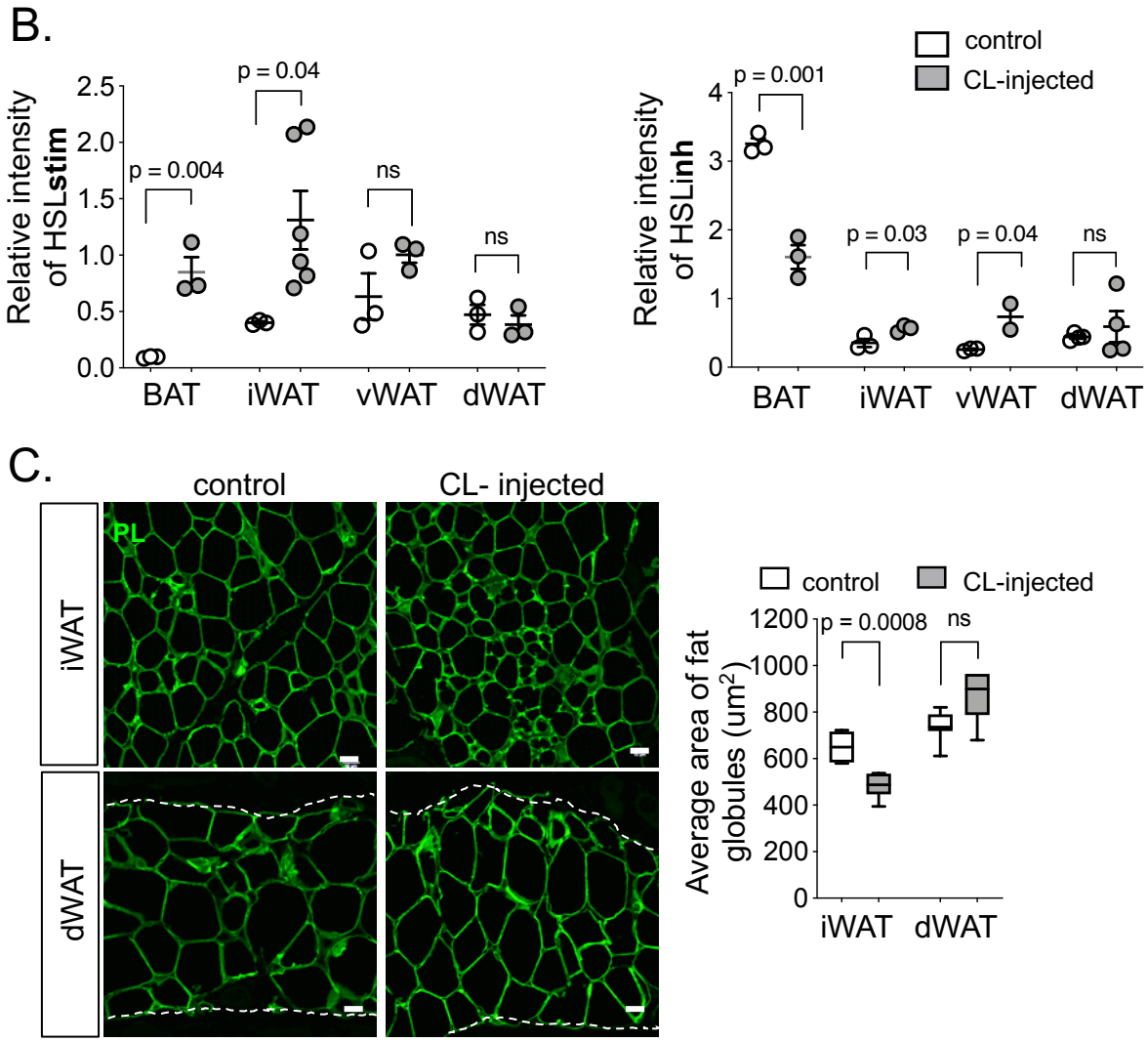

Fig. 5. Mouse dWAT is entirely insensitive to β-adrenergic lipolysis. A. *HSL and mTOR are not activated in dWAT by treatment with a β-adrenergic agonist.* Fat depots (brown adipose tissue, BAT; iWAT, vWAT and dWAT) were harvested from mice, euthanized 60 minutes after administration of CL (control n=5 and treated n=4). Immunofluorescent assay of regulatory modifications of hormone-sensitive lipase (HSL), either pS^{660} (pHSL stim) or pS^{565} (pHSL inh), or mTOR-activated S6 ($pS^{235/236}$) were quantified in **(B)** as described in Methods**.** Insets shown for pS6-stained dWAT show sebaceous glands (a, unstimulated; c, stimulated) and *panniculus carnosus* muscle layer (b, unstimulated; d, stimulated); scale bars=20 μm. **C.** *Fat stores of dWAT are not depleted after CL administration.* The size of lipid droplets (outlined by anti-perilipin staining) was assayed in dWAT and iWAT, 60 minutes after CL injection; scale bars=20 μm. Data were analyzed by unpaired two tailed *t* test.

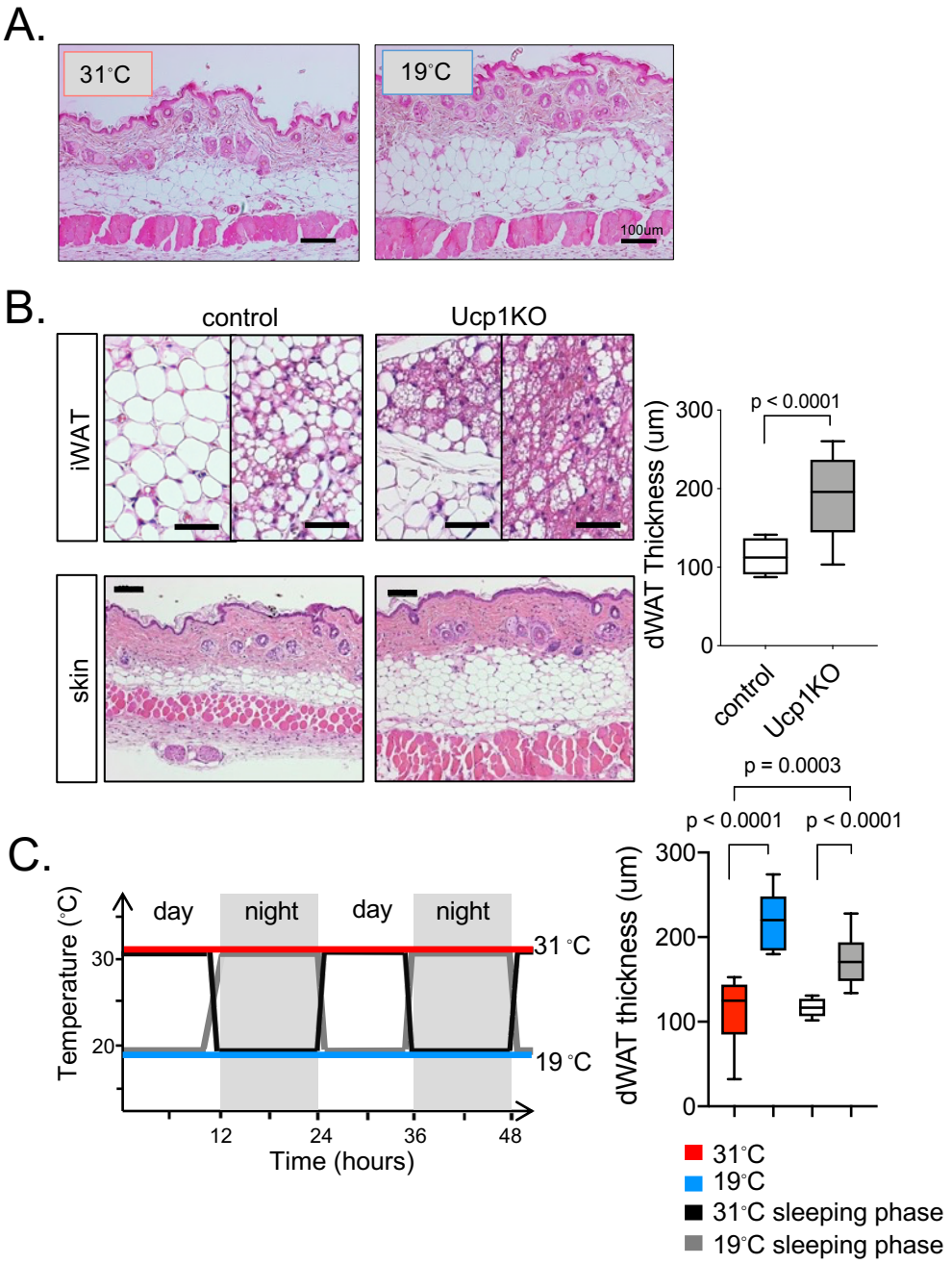

Fig. 6. Mouse dWAT accumulates when mice are challenged to produce heat. A. *dWAT thickens in response to sub-thermoneutral environmental housing*. dWAT thickness was assayed for mice housed at thermoneutrality (31^{0}C) or room temperature (19^{0}C) for 3 weeks; scale bars=100 μm. **B.** *dWAT thickens in UCP1-/- mice producing heat by non-canonical means.* H&E stained sections are shown for iWAT and dWAT from *UCP1-/-* or control C57BL/6J mice (10 to 19-week-old); quantified at right hand side. Scale bars=50 μm (iWAT) or 100 μm (skin). **C.** *Circadian cues promote dWAT accumulation.* Mice were housed individually with alternating circadian cycles of thermoneutral and room temperature housing for 3 weeks. The experimental paradigm is shown on the left, continuous warm (31^{0}C, red line), continuous cool (19^{0}C, blue line), or alternating daily cycles of warm sleeping /cool waking phases (black) or cool sleeping/warm waking phases (grey). The thickness of dWAT is shown on the right (n=5).

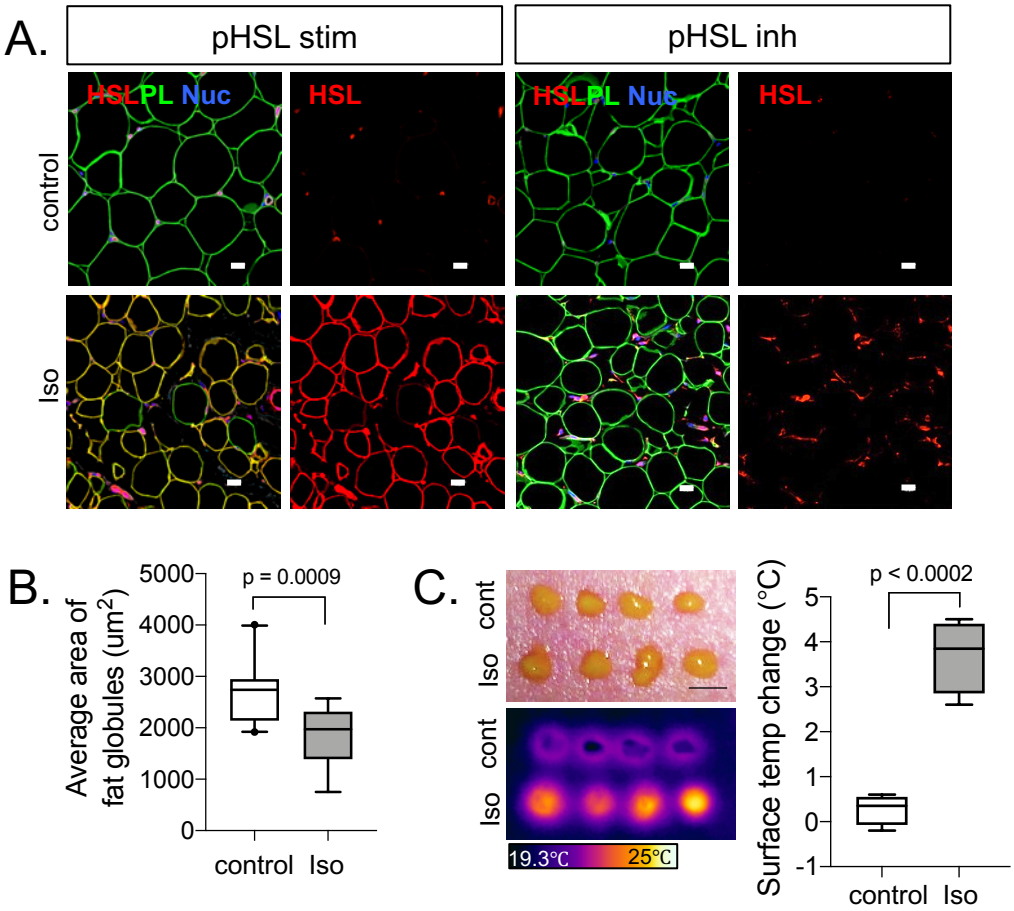

Fig. 7. Evaluation of β-adrenergic lipolytic response for human skin-associated fat depots. A. *Human skin associated adipocytes all respond to β-adrenergic agonists.* Immunofluorescent stains of pHSL stim and pHSL inh in sections of skin-associated fat from thigh, exposed to isoproterenol (Iso) *ex vivo,* counterstained with perilipin (PL) and DAPI (nuc; nuclei) (n=3). Scale bars=20 μm. **B.** *Human skin associated adipocytes are depleted by thermogenesis.* The average size of lipid droplets was quantified for the adipocytes visualized in A. **C.** *Human skin associated fat makes heat upon treatment with β-adrenergic agonist.* Infrared thermographic images of freshly collected fat capsules, pre-treated or not with isoproterenol for 40 mins, were quantified (right hand side). Scale bar=5mm. Data were analyzed using an unpaired 2-tailed t test.

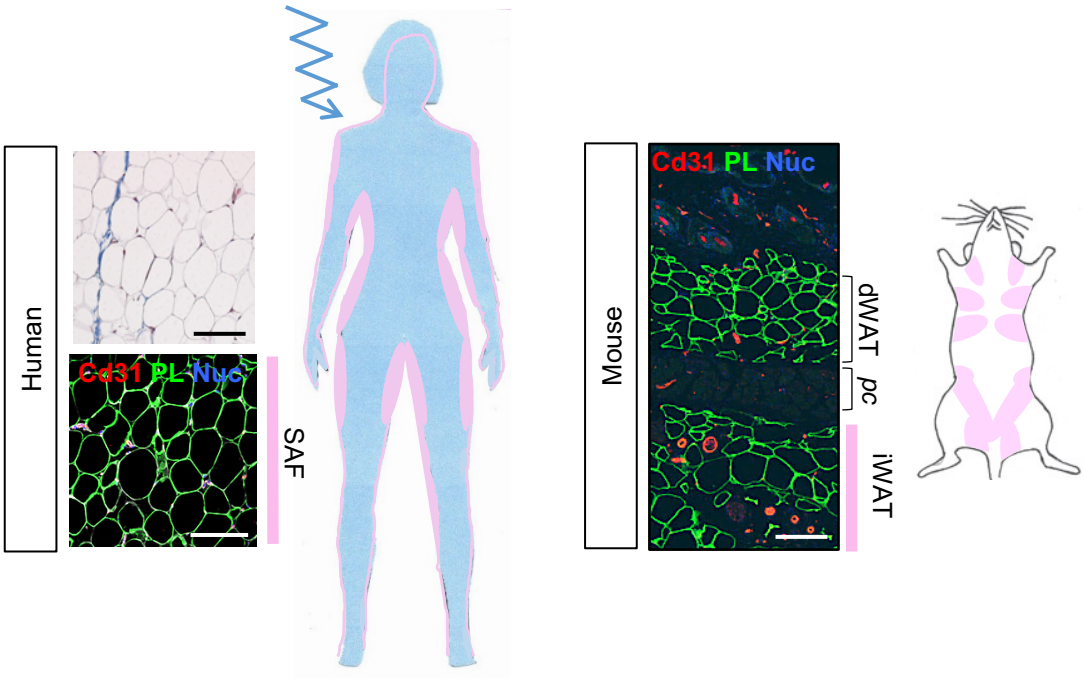

Fig. 8. Summary of inferred functionality of skin-associated adipose depots for human and mouse. In human (left hand side), the skin-associated fat depot is responsive to β-adrenergic demand and contributes heat towards body temperature homeostasis. For mouse (right hand side), there is a bilaminar adipose depot, the superficial dWAT layer is non-responsive to β-adrenergic demand (increasing insulative properties), whereas the subjacent iWAT depots are responsive. Immunofluorescent stained sections (both human and mouse) are stained for endothelial cells (CD31), perilipin (PL) and DAPI (nuc; nuclei); scale bars=100 μm.